19. Barber, G. A. Observations on the mechanisms of the reversible epimerization of GDP-D-mannose to GDP-L-galactose by an enzyme from *Chlorella pyrenidosa*. *J. Biol. Chem.* **254,** 7600–7603 (1979).
20. Barber, G. A. Synthesis of L-galactose by plant enzyme systems. *Arch. Biochem. Biophys.* **147,** 619–623 (1971).
21. Feingold, D. S. in *Encyclopedia of Plant Physiology*, Vol. 13A (eds Loewus, F. A. & Tanner, W.) 3–76 (Springer, Berlin, 1982).
22. Roberts, R. M. & Harrer, E. Determination of L-galactose in polysaccharide material. *Phytochemistry* **12,** 2679–2682 (1973).
23. Harris, G. C. *et al.* Mannose metabolism in corn and its impact on leaf metabolites, photosynthetic gas exchange, and chlorophyll fluorescence. *Plant Physiol.* **82,** 1081–1089 (1986).
24. Conklin, P. L., Williams, E. H. & Last, R. L. Environmental stress sensitivity of an ascorbic acid-deficient *Arabidopsis* mutant. *Proc. Natl Acad. Sci. USA* **93,** 9970–9974 (1996).
25. Conklin, P. L., Pallanca, J. E., Last, R. L. & Smirnoff, N. L-Ascorbic acid metabolism in the ascorbate-deficient *Arabidopsis* mutant *vtc1*. *Plant Physiol.* **115,** 1277–1285 (1997).
26. Chen, Y-T., Isherwood, F. A. & Mapson, L. W. Quantitative estimation of ascorbic acid and related substances in biological extracts by separation on a paper chromatogram. *Biochem. J.* **55,** 821–823 (1953).
27. Andrews, M. A. Capillary gas-chromatographic analysis of monosaccharides: improvements and comparisons using trifluoroacetylation and trimethylsilylation of sugar O-benzyl and O-methyl oximes. *Carbohydrate Res.* **194,** 1–19 (1989).
28. Ghebragzabher, M., Ruffini, S., Monaldi, B. & Lato, M. Thin layer chromatography of monosaccharides. *J. Chromatogr.* **127,** 133–162 (1976).
29. Dawson, R. M. C., Elliott, D. C., Elliott, W. H. & Jones, K. M. (eds) *Data for Biochemical Research* 2nd edn. (Clarendon, Oxford, 1969).

Acknowledgements. The research was supported by a BBSRC studentship (G.L.W.), a Nuffield Student Bursary (M.A.J.) and Zeneca Agrochemicals. We thank Nippon-Roche for the gift of L-sorbosone. Earlier work by J. Pallanca, funded by the BBSRC BOMRIP programme, provided a basis for this research. We thank M. Raymond for technical assistance; J. Kingdon and J. Hindley for growing the plants; and W. Schuch for his support.

Correspondence and requests for materials should be addressed to N.S. (e-mail: N.Smirnoff@exeter.ac.uk).

Visual input evokes transient and strong shunting inhibition in visual cortical neurons

Lyle J. Borg-Graham, Cyril Monier & Yves Frégnac

Equipe Cognisciences, Institut Alfred Fessard, CNRS, Avenue de la Terrasse, 91198 Gif sur Yvette, France

The function and nature of inhibition of neurons in the visual cortex have been the focus of both experimental and theoretical investigations[1–7]. There are two ways in which inhibition can suppress synaptic excitation[2,8]. In hyperpolarizing inhibition, negative and positive currents sum linearly to produce a net change in membrane potential. In contrast, shunting inhibition acts nonlinearly by causing an increase in membrane conductance; this divides the amplitude of the excitatory response. Visually evoked changes in membrane conductance have been reported to be nonsignificant or weak, supporting the hyperpolarization mode of inhibition[3,9–12]. Here we present a new approach to studying inhibition that is based on *in vivo* whole-cell voltage clamping. This technique allows the continuous measurement of conductance dynamics during visual activation. We show, in neurons of cat primary visual cortex, that the response to optimally orientated flashed bars can increase the somatic input conductance to more than three times that of the resting state. The short latency of the visually evoked peak of conductance, and its apparent reversal potential suggest a dominant contribution from γ-aminobutyric acid ((GABA)$_A$) receptor-mediated synapses. We propose that nonlinear shunting inhibition may act during the initial stage of visual cortical processing, setting the balance between opponent 'On' and 'Off' responses in different locations of the visual receptive field.

In the visual cortex, there are two major types of receptive fields, 'simple' and 'complex', based partly on the degree of spatial overlap between On and Off responses (evoked by an increase or decrease in light contrast, respectively) in the visual field[4,13]. Simple receptive fields have distinct On and Off subfields, whereas these are overlapping in complex cells. We can consider how intracortical inhibition works during visual cortical processing at different levels. At the functional level, inhibition could help in the push–pull organization of opponent responses (for example, hyperpolarization is evoked by a decrease in light contrast in the On subfield) seen in simple receptive fields[4]. It could also control the spatial tuning of On and Off excitation, as intracortical blockade of γ-aminobutyric acid $(GABA)_A$ receptors results in loss of segregation of On and Off excitatory responses in simple cells, whether measured extracellularly[1] or intracellularly[14].

At the biophysical level, even if shunting inhibition does exist, there is still a quantitative issue concerning its functional importance. As the reversal potential for $GABA_A$-mediated channels, which are probably responsible for the shunt in membrane conductance, is near the resting potential, shunting inhibition must produce a large change in the postsynaptic conductance to significantly counteract excitation. Simulations show that this shunt should be visible as a 100–200% increase in the somatic input conductance, $G_{in}(t)$, relative to the no-stimulus condition (characterized as G_{rest})[2,15]. However, measurements from current clamp recordings have indicated limited conductance changes (relative

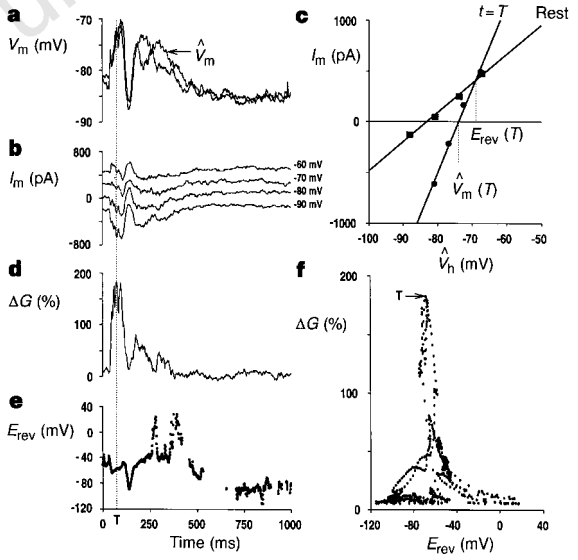

Figure 1 The visually evoked relative change in input conductance $\Delta G_{in}(t)$ and its apparent reversal potential $E_{rev}(t)$ are derived from the current waveforms measured by two to four voltage-clamp protocols, illustrated here for the subthreshold response of an end-stopped simple cell to an Off transition of a flashing bar (full response is shown in Fig. 2e, cell 4, position 8). **a**, Voltage responses under current clamp and predicted $\hat{V}_m$ (arrow) from voltage-clamp currents, assuming a linear model. **b**, Responses under voltage clamp for four command holding potentials. **c**, *I/V* characteristics derived from linear regressions corresponding to the resting state (squares), the slope of which gives G_{rest}, and during visual activation (circles) at the time T marked by a dotted line in (**a**–**e**), the slope of which gives $G_{in}(T)$. The voltage axis, $\hat{V}_h$, corresponds to the command holding potential corrected for R_s. The interpolated voltage at zero current of the *I/V* characteristic at any given time predicts the current clamp response ($\hat{V}_m(t)$ in **c**. The stability of the recording, and the justification of a linear approximation for this subthreshold example, are shown by the close match between the original and the interpolated traces superimposed in **a**. **d**, Relative $\Delta G_{in}(t)$, derived continuously over the complete duration of the visual stimulation. **e**, $E_{rev}(t)$. **f**, Phase plot of relative $\Delta G_{in}(t)$ versus $E_{rev}(t)$, where each point represents averages taken over 1 ms, illustrating the various trajectories in time (arrow for time T). In this case, the conductance response at time 0 is >105% of the input conductance at rest because the tail of the On response starts 1000 ms earlier. All responses in this paper are averages of 10 trials.

$\Delta G_{in}(t)$ typically in the order of 5–20%) during optimal and non-optimal visual activation[3,8–11].

We aimed to examine the balance between the excitation and inhibition underlying the spatial opponency of On and Off responses, and to identify the biophysical nature of the inhibition, using a new method for the continuous measurement of conductance dynamics. The standard approach to characterize $G_{in}(t)$ (used in the visual cortex *in vitro*[16,17] and *in vivo*[9,12,18]) is to measure voltage deflections in response to injected current pulses. A major constraint of this method is that although the rate of repetition of the pulses should be at least twice the highest frequency in the conductance signal, the pulse rate is limited by the resting time constant to account for the capacitive component of the input impedance. Voltage-dependent channels activated by the voltage change during a current pulse or by action potentials, and the electrical shunt introduced by sharp microelectrodes, also tend to underestimate the relative $\Delta G_{in}(t)$. Another approach[10] relies on measuring the amplitude of electrically evoked test excitatory postsynaptic potentials (EPSPs) during the visual response. However, as the peak of the EPSP is reached within a few milliseconds, its amplitude approaches that of the peak response to a current impulse delivered at the soma, in this case given by the ratio of the EPSP driving force and cell capacitance. Thus, this technique is an insensitive measure of $\Delta G_{in}(t)$.

To overcome these constraints, we derived the entire $\Delta G_{in}(t)$ waveform from whole-cell, steady-state, voltage-clamp recordings. After characterization of receptive fields under current clamp (see, for example, Fig. 1a), we repeated the measurements of the response to the same visual stimulus under voltage clamp (continuous mode, no compensation for the access resistance, R_s) at two to four holding potentials, V_h (Fig. 1b). We then derived $G_{in}(t)$, where time is referenced to the visual stimulus, from the slope of the linear regression (*I/V* characteristic) of the points given by the measured averaged current, $I_m(t)$, and the holding potential, $\hat{V}_h$, corrected for the drop across R_s ($\hat{V}_h(t) = V_h(t) - R_s \times I_m(t)$) (Fig. 1c). The relative $\Delta G_{in}(t)$ was then taken as $100 \times (G_{in}(t) - G_{rest})/G_{rest}$(%) (Fig. 1d).

As with any somatic-based impedance measurement, this method does not overcome the loss of visibility of dendritic inputs due to synaptic interactions or cable attenuation, or contamination by currents from poorly clamped voltage-dependent dendritic membrane[19,20]. Rather, the advantage of using the voltage-clamp method is that distortion of synaptic events by transient voltage-dependent channels and capacitance near to the recording site are minimized. This method also allows the continuous estimation of the apparent somatic reversal potential of the visual response, $E_{rev}(t)$. This value is taken as the voltage of the intersection between the *I/V* characteristic at every time *t* and at rest (Fig. 1e) whenever the relative difference in their slopes (that is, relative $\Delta G_{in}(t)$) was

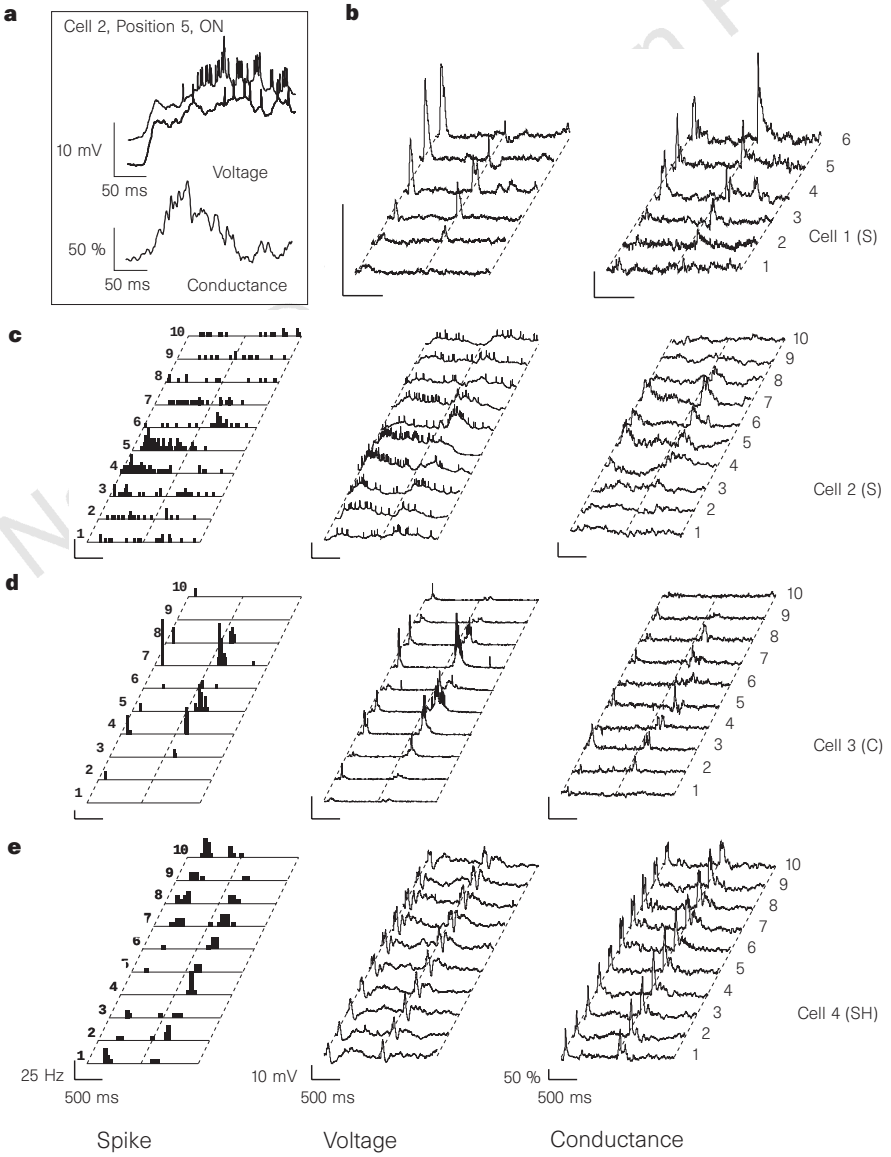

Figure 2 Response–plane receptive field maps based on spike activity (peri-stimulus histograms, PSTHs, left column), voltage (centre) and conductance (right) measurements. **a**, Time course of the voltage responses (top, 100 pA and bottom, 0 pA injected current) and of the conductance observed for the dominant On response of cell 2 in position 5. **b**–**e**, Response–plane maps for two simple cells (cells 1, 2, **b**, **c**) one complex cell (cell 3, **d**) and one end-stopped simple cell (cell 4, **e**). Stimuli are optimally oriented light bars flashed On and Off during two consecutive periods of 1 s, in adjacent locations in the visual field, spaced by 0.7° for cell 1, 0.5° for cell 2, and 1° for cells 3 and 4. For cell 4, a long bar stimulus was used to emphasize the inhibitory response. PSTHs are shown in the absence (**b**, **d**) or presence (**c**, **e**) of a constant depolarizing current (100 pA in **c**, 300 pA in **e**). G_{rest} and R_s values were, respectively, 17 nS and 60 MΩ for cell 1, 40 nS and 25 MΩ for cell 2, 15 nS and 20 MΩ for cell 3, and 29 nS and 15 MΩ for cell 4. Horizontal scale, 500 ms; vertical scales, 25 action potential per second for the PSTHs, 10 mV for the voltage traces, and 50% for relative $\Delta G_{in}(t)$.

>5%. This criterion allows a precise determination of the intersection point of the two characteristics. Assuming that the change in the visually evoked somatic conductance reflects the composite synaptic input reaching the soma, $E_{rev}(t)$ characterizes the balance between excitation and inhibition over time. Finally, to indicate more clearly the type of synaptic input underlying the conductance changes, we constructed phase plots of the relative $\Delta G_{in}(t)$ against $E_{rev}(t)$ (Fig. 1f).

The recordings from seven cells, from a total population of 109 cells first characterized in current clamp (see Methods), were stable enough in terms of R_s and visual responsiveness to allow reliable measurement of both visually evoked voltages and synaptic currents in receptive fields (response-plane maps[21]). Previous studies of On/Off opponency have concluded, on a qualitative basis, that the dominant and opponent responses in simple cells result from pure excitation and from pure subtractive inhibition, respectively[4,9,22,23]. However, comparison of the temporal profiles of the post-stimulus time histograms (PSTHs), and the averaged evoked synaptic potential under current clamp, shows that both types of response in simple cells (Fig. 2b, c) may include composite excitatory/inhibitory input (for example, in Fig. 2c the dominant response in cell 2 position 5, and in Fig. 2b the opponent responses in cell 1, positions 5 and 6).

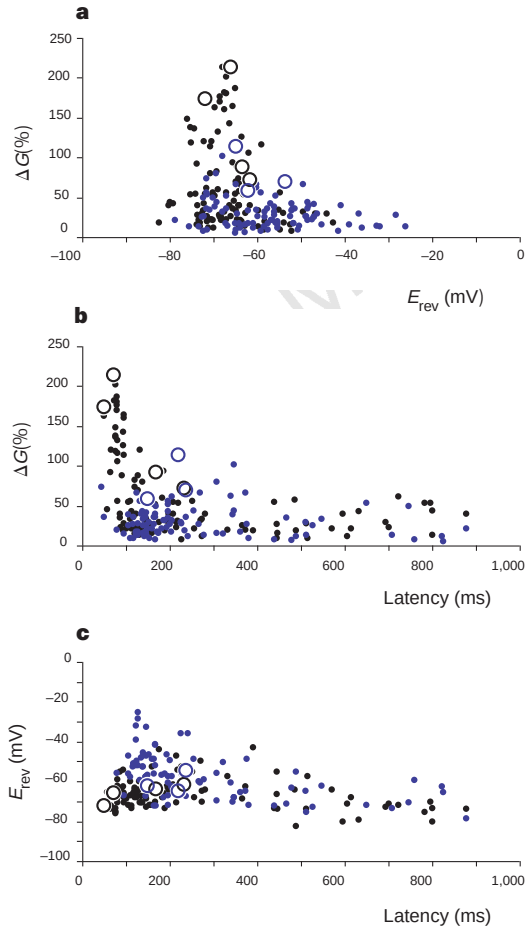

Figure 3 Relationships between amplitude, latency and apparent reversal potential of the maximum values of relative $\Delta G_{in}(t)$. Each point in the graphs corresponds to one stimulus condition (On or Off light or dark bar flashed at a given position). Results from seven cells (11 protocols) for all tested positions have been pooled. The responses with the maximum value of the relative $\Delta G_{in}(t)$ for each cell are marked by open circles. Black and blue symbols refer to simple and complex cells, respectively. **a**, Maximal ΔG versus E_{rev}. **b**, Maximal ΔG versus latency. **c**, E_{rev} versus latency.

The conductance profiles derived from the voltage-clamp measurements show that, for a given position in the receptive field, On and Off stimuli trigger a similar transient increase of $G_{in}(t)$ (Fig. 2). The average value for the largest relative conductance increases seen in each cell was 113% (s.d. = 58%, $n = 7$; see Fig. 3). In general, the maximum and global shape of the $\Delta G_{in}(t)$ waveform did not parallel the overall spike output or the waveform of the voltage record (see, for example, positions 5–6 for cell 1 in Fig. 2b, and positions 5–7 for cell 2 in Fig. 2c). Detailed examination shows that the rising phase and maximum of the conductance peaks are associated with an absence of spikes for both dominant and opponent responses, even when applying a depolarizing current to increase the cell's responsiveness (Fig. 2a, inset), indicating a transient early suppressive effect. The largest peaks (138% ± 69%, $n = 4$) were observed for three simple cells and one end-stopped simple cell (Figs 2b, c, e and 4). Three complex cells showed smaller but still significant conductance transients (80% ± 29%, $n = 3$; Figs 2d and 4).

Phase plots for relative $\Delta G_{in}(t)$ versus $E_{rev}(t)$ indicate a prototypical bounded region for the synaptic dynamics that is independent both of the resting potential of the cell and of its functional type (Fig. 4). The extrapolated E_{rev} peak values of all state trajectories converge near −60 to −70 mV. The averaged value of the actual peaks established for all seven cells (− 63.3 mV ± 5.5 mV), when compared to the reversal potentials of the major classes of currents gated by excitatory and inhibitory transmitters, concurs with the $GABA_A$ reversal potential measured *in vitro* with identical patch pipette solutions (− 64 ± 9 mV) (ref. 24). The main difference in the trajectories associated with specific On or Off responses is that, typically, more positive potentials were produced when the preferred stimulus was present (for example, the On response in position 6 for cell 1 and position 7 for cell 3; see Fig. 4), and more negative potentials were produced in response to both preferred and opponent stimuli (for example, cell 4 in Fig. 4e), indicating $GABA_B$ receptor activation[16]. The trajectories often reached E_{rev} values beyond those expected for either $GABA_B$ (less than −90 mV) or α-amino-3-hydroxy-5-methyl-4-isoxazole propionic acid (AMPA) (>0 mV), which can be accounted for by voltage escape of distal inputs[20]. The early onset of the larger conductance peaks, occurring sometimes as early as 50–70 ms after stimulation (Fig. 3b), further supports the conclusion that these responses are dominated by $GABA_A$ rather than $GABA_B$ activation ($GABA_B$ activation occurs after longer latencies[16]). In some cases, early excitatory input is subsequently shunted by the large inhibitory input, with E_{rev} moving rapidly to a value close to the $GABA_A$ reversal potential (Fig. 4a, chronogram inset). The consistent shape of the phase plots has two possible interpretations, not mutually exclusive. First, shunting inhibition is the largest component of synaptic activation that reaches the soma. Second, the shape of the peak may be constrained by the relative visibility at the soma of proximal $GABA_A$ inputs compared with more distal excitatory (and perhaps $GABA_B$) inputs[15,25].

These findings are consistent with the two following observations. First, synaptic excitation and inhibition seem to overlap strongly during visual activation[5,26] as is the case when synaptic activation is produced by electrical activation of thalamic or intracortical axons *in vitro*[16] and *in vivo*[18]. Second, both electrical stimulation of intracortical pathways and iontophoretically applied GABA evoke a significant conductance increase *in vitro* as well as *in vivo*[14,16,18], contradicting the suggestion that, whatever the mode of activation, the effects of inhibition *in vivo* should differ from those obtained *in vitro*[17].

These results argue against an extreme schematization of the synaptic basis for the spatial discreteness of On and Off subfields and opponency of their On and Off spike responses, according to which each subfield in simple cells is constructed exclusively from either On excitation only and Off inhibition only in On regions, or

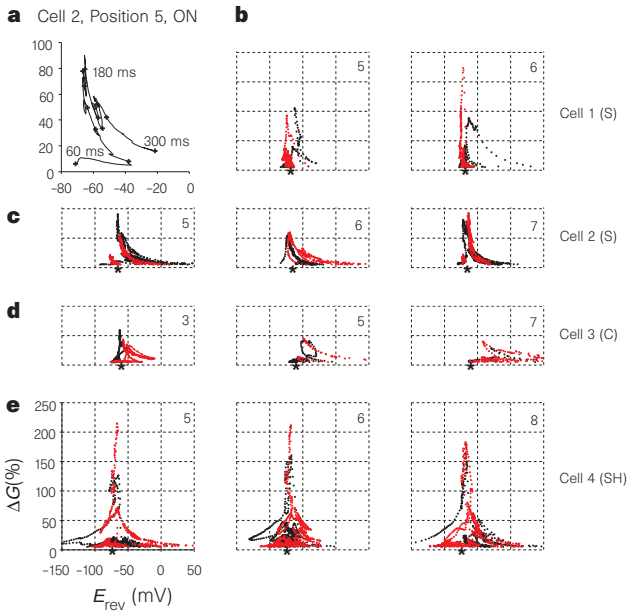

Figure 4 Phase plots of relative $\Delta G_{in}(t)$ versus $E_{rev}(t)$ for positions in the receptive fields (indicated in corner of each graph) eliciting the largest conductance or spike responses. **a**, The chronogram corresponds to the first 300 ms of the dominant response (0 nA) detailed in Fig. 2a. **b**–**e**, Plots correspond to the same cells shown in Fig. 2b–e. Asterisks under the plots indicate the cells' resting potentials (–76 mV for cell 1, –74 mV for cell 2, –68 mV for cell 3 and –80 mV for cell 4). Black and red dots correspond to the On and Off responses, respectively.

vice versa[4,13]. Rather, the profiles of $E_{rev}(t)$ for dominant and opponent responses, and the study of synaptic responses under bicuculline application[14], indicate that both On and Off responses normally combine excitatory and inhibitory inputs. We propose that excitatory and inhibitory synaptic inputs interact to shape the response for each On or Off transition of the stimulus by controlling the global gain of the cortical spiking response. A strongly shunting $GABA_A$ input would be decisive during an early, nonlinear step of processing, allowing the dynamic emergence of the On/Off opponency expressed by small networks of reciprocally connected simple cells. If this shunting priming signal is weak, these circuits would then operate in a complex-like mode that lacks this form of functional selectivity. □

Methods

We recorded cells in the primary visual cortex of anaesthetized (Althesin), paralysed kittens and adult cats as described[26,27]. For data-processing and visual-stimulation protocols we used in-house software. Patch electrode (3–5 MΩ) solutions contained 140 mM K-gluconate, 10 mM HEPES, 4 mM ATP, 2 mM $MgCl_2$, 0.4 mM GTP and 0.5 mM EGTA (KOH), with pH adjusted to 7.3 and the osmolarity adjusted to 285 mosM. We obtained whole-cell patch recordings (Axoclamp 2A amplifier) to depths ≤2,000 μm. The estimate of R_s was revised as necessary over the course of the experiment and, in some cases, off-line by fitting the response to subthreshold hyperpolarizing current steps to the sum of two exponentials, with the faster exponential corresponding to the contribution of the electrode. Estimation of R_s was also confirmed by equalization of the height of the initial spike in response to different strengths of sustained depolarizing current. No significant correlation was found between R_s and the peak value of $G_{int}(t)$. We measured a tip offset potential of 10 mV, which was subtracted from the voltage records off-line[28].

We characterized electrophysiological and receptive-field properties under current clamp for 109 cells, each of which was recorded for >10 min (mean ± s.d. = 35 ± 26 min, range 11–146 min), seal resistance in attached mode $R_{seal} > 2$ GΩ (3.7 ± 1.6 GΩ, range 2–10 GΩ), and $R_s < 60$ MΩ (22 ± 15 MΩ, range 4–60 MΩ). In these cells the average input resistance R_{in} was 84.8 MΩ (±64.3 MΩ, range 14–320 MΩ), the average membrane time constant τ_0 was 14.3 ms (±12.4 ms), and the average resting potential was –72.8 mV (±9 mV).

We determined principal On and Off fields first by hand under current clamp using moving bars whose dimensions were adjusted to maximize firing, and then quantitatively by flashing optimally oriented bars (width 0.1–1.0 degrees) of both positive and negative contrasts at ten adjacent non-overlapping positions across the receptive field. Visual-stimulation protocols were begun 10–15 minutes after whole-cell access, and lasted typically for 1 h. Receptive fields were classified as simple or complex on the basis of spike activity[27,29]. In the case of reduced levels of visually evoked firing (see, for example, Fig. 2b), we classified a subfield as simple when there was a clear opponent hyperpolarization in the voltage record[4].

Received 14 October 1997; accepted 2 March 1998.

1. Sillito, A. M. The contribution of inhibitory mechanisms to the receptive field properties of neurones in striate cortex of the cat. *J. Physiol.* **250,** 305–329 (1975).
2. Koch, C. & Poggio, T. in *Models of the Visual Cortex* (eds Rose, D. & Dobson, V. G.) 408–419 (J. Wiley and Sons, Chichester, 1985).
3. Douglas, R. J., Martin, K. A. C. & Whitteridge, D. Selective responses of visual cortical cells do not depend on shunting inhibition. *Nature* **332,** 642–644 (1988).
4. Ferster, D. Spatially opponent excitation and inhibition in simple cells of the cat visual cortex. *J. Neurosci.* **8,** 1172–1180 (1988).
5. Volgushev, M., Pei, X., Vidyasagar, T. R. & Creutzfeldt, O. D. Excitation and inhibition in orientation selectivity of cat visual cortex neurons revealed by whole-cell recordings *in vivo*. *Vis. Neurosci.* **10,** 1151–1155 (1993).
6. Bush, P. C. & Sejnowski, T. J. Effects of inhibition and dendritic saturation in simulated neocortical pyramidal cells. *J. Neurophys.* **71,** 2183–2193 (1994).
7. Carandini, M. & Heeger, D. J. Summation and division by neurons in primate visual cortex. *Science* **264,** 1333–1336 (1994).
8. Eccles, J. C. *The Physiology of Synapses* (Springer, Berlin, 1964).
9. Berman, N. J., Douglas, R. J., Martin, K. A. C. & Whitteridge, D. Mechanisms of inhibition in cat visual cortex. *J. Physiol.* **440,** 697–722 (1991).
10. Ferster, D. & Jagadeesh, B. EPSP-IPSP interactions in cat visual cortex studied with *in vivo* whole-cell patch recording. *J. Neurosci.* **12,** 1262–1274 (1992).
11. Carandini, M. & Ferster, D. A tonic hyperpolarization underlying contrast adaptation in cat visual cortex. *Science* **276,** 949–952 (1997).
12. Pei, X., Volgushev, M., Vidyasagar, T. R. & Creutzfeldt, O. D. Whole-cell recording and conductance measurements in cat visual cortex *in vivo*. *Neuroreport* **2,** 485–488 (1991).
13. Hubel, D. H. & Wiesel, T. N. Receptive fields, binocular interaction and functional architecture in the cat's visual cortex. *J. Physiol.* **160,** 106–154 (1962).
14. Shulz, D., Bringuier, V. & Frégnac, Y. Complex-like structure of simple visual cortical receptive fields is masked by $GABA_A$ intracortical inhibition. *Soc. Neurosci. Abstr.* **19,** 638 (1993b).
15. Koch, C., Douglas, R. & Wehmeier, U. Visibility of synaptically induced conductance changes: theory and simulations of anatomically characterized cortical pyramidal cells. *J. Neurosci.* **10,** 1728–1744 (1990).
16. Connors, B. W., Malenka, R. C. & Silva, L. R. Two inhibitory postsynaptic potentials and $GABA_A$ and $GABA_B$ receptor mediated responses in neocortex of rat and cat. *J. Physiol.* **406,** 443–468 (1988).
17. Berman, N. J., Douglas, R. J. & Martin, K. A. C. The conductances associated with inhibitory postsynaptic potentials are larger in visual cortical neurones *in vitro* than in similar neurones in intact, anaesthetized rats. *J. Physiol.* **418,** 107 (1989).
18. Dreifuss, J. J., Kelly, J. S. & Krnjevic, K. Cortical inhibition and gamma-aminobutyric acid. *Exp. Brain Res.* **9,** 137–154 (1969).
19. Rall, W. in *Neural Theory and Modeling* (ed. Reiss, R. F.) 73–97 (Stanford Univ., 1964).
20. Spruston, N., Jaffe, D. B., Williams, S. H. & Johnston, D. Voltage- and space-clamp errors associated with the measurement of electronically remote synaptic events. *J. Neurophys.* **70,** 781–802 (1993).
21. Palmer, L. A. & Davis, T. A. Receptive field structure in cat striate cortex. *J. Neurophys.* **46,** 260–295 (1981).
22. Jagadeesh, B., Wheat, H. S. & Ferster, D. Linearity of summation of synaptic potentials underlying direction sleectivity in simple cells of the cat visual cortex. *Science* **262,** 1901–1904 (1993).
23. Nelson, S., Toth, L., Sheth, B. & Sur, M. Orientation selectivity of cortical neurons during intracellular blockade of inhibition. *Science* **265,** 774–777 (1994).
24. Barker, J. L. & Harrison, N. L. Outward rectification of inhibitory postsynaptic currents in cultured rat hippocampal neurones. *J. Physiol.* **403,** 41–55 (1988).

25. Anderson, J. C., Douglas, R. J., Martin, K. A. C. & Nelson, J. C. Map of the synapses formed with the dendrites of spiny stellate neurons of cat visual cortex. *J. Comp. Neurol.* **341,** 25–38 (1994).
26. Bringuier, V., Frégnac, Y., Baranyi, A., Debanne, D. & Shulz, D. Synaptic origin and stimulus dependency of neuronal oscillatory activity in the primary visual cortex of the cat. *J. Physiol.* **500,** 751–774 (1997).
27. Debanne, D., Shulz, D. & Frégnac, Y. Activity-dependent regulation of ON and OFF responses in cat visual cortical receptive fields. *J. Physiol.* **500,** 523–548 (1998)..
28. Neher, E. in *Methods in Enzymology: Ion Channels* (eds Rudy, B. & Iverson, L. E.) 123–131 (Academic, New York, 1992).
29. Orban, G. A. *Neuronal Operations in the Visual Cortex* (Springer, Berlin, Heidelberg, 1984).

Acknowledgements. We thank V. Bringuier and F. Chavane for help with some experiments; N. Gazeres, T. Bal, K. Grant, R. Kado, P.-M. Lledo, N. Ropert and D. Shulz for comments; and G. Sadoc and L. Glaeser for software assistance. This work was supported by HFSP and GIS Cognisciences grants (to Y.F.). L.J.B.G. was funded by fellowships from the CNRS and Foundations Philippe and Fyssen.

Correspondence and requests for materials should be addressed to Y.F. (e-mail: fregnac@iaf.cnrs-gif.fr).

Acute stress facilitates long-lasting changes in cholinergic gene expression

Daniela Kaufer*, Alon Friedman*†, Shlomo Seidman* & Hermona Soreq*

** Department of Biological Chemistry, The Alexander Silberman Life Sciences Institute, The Hebrew University of Jerusalem, Jerusalem 91904, Israel*
† Departments of Physiology and Neurosurgery, Faculty of Health Science, and Zlotowski Center for Neuroscience, Ben Gurion University, Beersheva 84105, Israel

Acute traumatic stress may lead to post-traumatic stress disorder (PTSD)[1], which is characterized by delayed neuropsychiatric symptoms including depression, irritability, and impaired cognitive performance[2]. Curiously, inhibitors of the acetylcholine-hydrolysing enzyme acetylcholinesterase may induce psychopathologies that are reminiscent of PTSD[3,4]. It is unknown how a single stressful event mediates long-term neuronal plasticity. Moreover, no mechanism has been proposed to explain the convergent neuropsychological outcomes of stress and of acetylcholinesterase inhibition. However, acute stress elicits a transient increase in the amounts released of the neurotransmitter acetylcholine and a phase of enhanced neuronal excitability[5]. Inhibitors of acetylcholinesterase also promote enhanced electrical brain activity[6], presumably by increasing the survival of acetylcholine at the synapse. Here we report that there is similar bidirectional modulation of genes that regulate acetylcholine availability after stress and blockade of acetylcholinesterase. These calcium-dependent changes in gene expression coincide with phases of rapid enhancement and delayed depression of neuronal excitability. Both of these phases are mediated by muscarinic acetylcholine receptors. Our results suggest a model in which robust cholinergic stimulation triggers rapid induction of the gene encoding the transcription factor c-Fos. This protein then mediates selective regulatory effects on the long-lasting activities of genes involved in acetylcholine metabolism.

The molecular mechanisms translating a traumatic life experience into long-term neuropsychological sequelae are expected to involve complex changes in gene regulation. We have previously shown that adult FVB/N mice subjected to either forced swimming stress or inhibitors of the acetylcholine-hydrolysing enzyme acetylcholinesterase (AChE) exhibit dramatic increases in levels of messenger RNA encoding the early immediate transcription factor c-Fos in the brain[7]. *In vitro*, sagittal corticohippocampal brain slices exposed to AChE inhibitors showed enhanced neuronal excitability and similar increases in cortical c-*fos* gene expression within 10 min (Fig. 1a). These increases are mediated by cholinergic stimulation of muscarinic acetylcholine receptors.

The presence of c-Fos-binding sites in the promoters of key cholinergic genes, such as the genes encoding AChE[8,9], the acetylcholine-synthesizing enzyme choline acetyltransferase (ChAT)[10], and the vesicular acetylcholine transporter (VAChT)[11], indicated that elevated c-Fos levels might activate regulatory pathway(s) leading to long-term changes in the expression of proteins mediating brain cholinergic neurotransmission. We performed quantitative reverse transcription with polymerase chain reaction (RT-PCR) on cortical RNA extracted either from mice 10–90 min after forced swimming or from brain slices after exposure to the cholinesterase

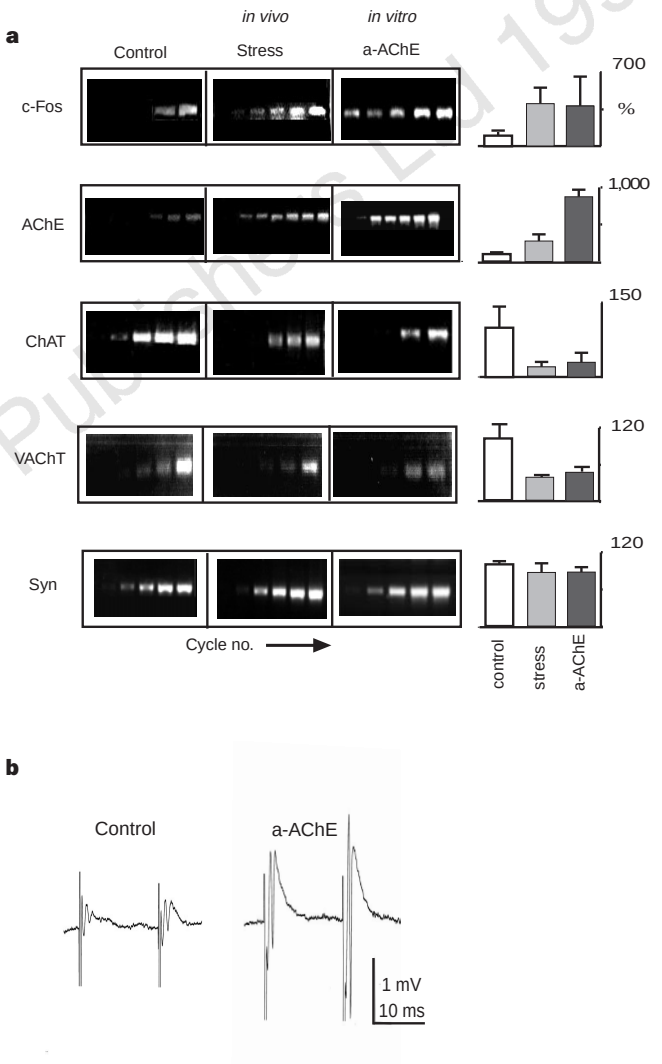

Figure 1 Acute stress and anticholinesterases modulate CNS gene expression similarly. **a**, RT-PCR analysis was performed on RNA extracted from the cortex of control mice and stressed mice or from sagittal corticohippocampal slices incubated with 1μM DFP or 1mM pyridostigmine (a-AChE). Products were sampled every third cycle, electrophoresed, and stained with ethidium bromide. Data reflect c-Fos mRNA levels 10 min after stress or AChE inhibition, and AChE, ChAT, VAChT and synaptophysin (Syn) RNA levels 30 min after treatment. The figure shows representative gels and relative band intensities (mean ± s.d.), calculated from densitometric analysis of a single cycle verified to be within the linear range of product accumulation for the specific PCR reaction. On average, five RNA samples were analysed for each treatment group. For c-Fos, AChE, ChAT and VAChT, the differences in RNA levels observed between the control and either stress or a-AChE samples were all found to be statistically significant ($P < 0.02$) in a two-tailed Student's *t*-test. RNA from non-treated control animals generated patterns similar to those from non-treated slices (not shown). **b**, AChE inhibition increases neuronal excitability. The figure shows extracellular evoked potentials recorded in the CA1 area before (control) or 30 min following (a-AChE) addition of 1μM DFP to the perfusing solution. One of five reproducible experiments.